



Dalton
Transactions

**EXAFS Investigations of Temperature-Dependent Structure
in Cobalt-59 Molecular NMR Thermometers**

Journal:	<i>Dalton Transactions</i>
Manuscript ID	DT-ART-04-2020-001391.R1
Article Type:	Paper
Date Submitted by the Author:	13-May-2020
Complete List of Authors:	Ozvat, Tyler; Colorado State University, Chemistry Sterbinsky, George ; Argonne National Laboratory Campanella, Anthony; Colorado State University System, Chemistry Rappe, Anthony; Colorado State University, Chemistry Zadrozny, Joseph; Colorado State University, Chemistry

SCHOLARONE™
Manuscripts

EXAFS Investigations of Temperature-Dependent Structure in Cobalt-59 Molecular NMR Thermometers

Received 00th January 20xx,
Accepted 00th January 20xx

Tyler M. Ozvat,^a George E. Sterbinsky,^b Anthony J. Campanella,^a Anthony K. Rappé,^a and Joseph M. Zadrozny*^a

DOI: 10.1039/x0xx00000x

Cobalt-59 nuclei are known for extremely thermally sensitive chemical shifts (δ), which in the long term could yield novel magnetic resonance thermometers for bioimaging applications. In this manuscript, we apply extended X-ray absorption fine-structure spectroscopy (EXAFS) for the first time to probe the exact variations in physical structure that produce the exceptional thermal sensitivity of the ^{59}Co NMR chemical shift. We apply the technique to five Co(III) complexes: $[\text{Co}(\text{NH}_3)_6]\text{Cl}_3$ (**1**), $[\text{Co}(\text{en})_3]\text{Cl}_3$ (**2**) (en = ethylenediamine), $[\text{Co}(\text{tn})_3]\text{Cl}_3$ (**3**) (tn = trimethylenediamine), $[\text{Co}(\text{tame})_2]\text{Cl}_3$ (**4**) (tame = 1,1,1-tris(aminomethyl)ethane), and $[\text{Co}(\text{diNOsar})]\text{Cl}_3$ (**5**) (diNOsar = dinitrosarcophagine). The solution-phase EXAFS data reveal increasing Co–N bond distances for these aqueous complexes over a $\sim 50^\circ\text{C}$ temperature window, expanding by $\Delta r_{(\text{Co-N})} = 0.0256(6)$ Å, $0.0020(5)$ Å, $0.0084(5)$ Å, $0.0006(5)$ Å, and $0.0075(6)$ Å for **1-5**, respectively. Computational analyses of the structural changes reveal that increased connectivity between the donor atoms encourages complex structural variations. These results imply that rich temperature-dependent structural variations define the ^{59}Co NMR thermometry in macrocyclic complexes.

Introduction

Magnetic resonance imaging (MRI) thermometry would enable minimally invasive thermal therapies to treat benign and malignant disease.^{1–5} In order to develop applicable molecular probes for this technology, it is essential to understand how to program variable-temperature MR properties via molecular structure design. ^{59}Co is a promising nucleus for developing this technology as it has a stronger temperature-dependent chemical shift ($\Delta\delta/\Delta T$) than any other nucleus in a closed-shell molecule and an enormous (~ 18000 ppm-wide) chemical shift window.^{6,7} These advantages are coupled with numerous others for the ^{59}Co isotope, including a relatively high nuclear magnetic moment ($I = 7/2$, $\mu = 4.62 \mu_N$), 100% natural abundance, and high receptivity (0.278 relative to ^1H).⁸ Hence, the nucleus is worth of considerable further investigation.

The present record for temperature sensitivity of the ^{59}Co chemical shift $\Delta\delta/\Delta T$ is $3.15 \text{ ppm}/^\circ\text{C}$ for $\text{Co}(\text{acac})_3$.⁹ Toward eventual *in vivo* utility, it is necessary to develop design principles for higher $\Delta\delta/\Delta T$ values. Furthermore, owing to the toxicity of free cobalt ions in the body,¹⁰ and the desire for an MR probe to maintain functionality, design strategies should ideally harness macrocyclic ligands that yield extremely stable complexes. With these points in mind, we recently reported

that $\Delta\delta/\Delta T$ for the ^{59}Co nucleus is enhanced for macrocyclic chelates as opposed to mono- or bidentate ligands.¹¹

Theoretical models of temperature sensitivity in transition-metal NMR decades ago proposed that $\Delta\delta/\Delta T$ stems from expansions of M–L bonds (Fig. 1).^{12–17} In this light, the observed enhancement of $\Delta\delta/\Delta T$ for a macrocyclic ligand¹¹ over mono- or bidentate ligands is counterintuitive, as the rigid structure is envisioned to resist M–L expansion. However, temperature-dependent changes in bond distance for a macrocycle should also induce changes to M–L bond angles. Hence, relatively complex structural changes, including changes to N–Co–N bond

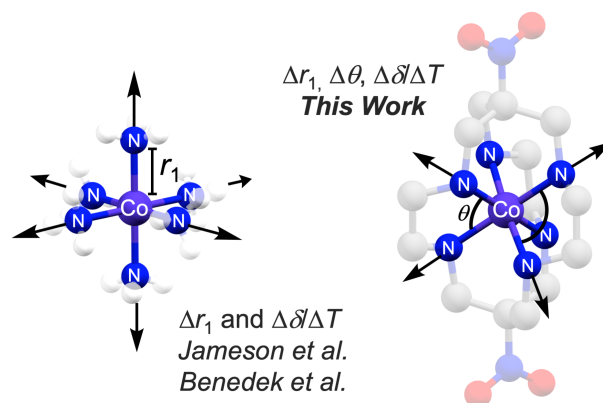


Fig. 1. Initial models by Jameson et al.^{12,13} and Benedek et al.¹⁴ rationalize ^{59}Co $\Delta\delta/\Delta T$ on the basis of coordination-geometry expansion (Δr_1 , above). In this paper we use EXAFS spectroscopy to test the contribution(s) of bond expansion to $\Delta\delta/\Delta T$. Faded blue, red, gray, and white spheres represent N, O, C, and H atoms in the ligand backbones for the shown molecules.

^a Department of Chemistry, Colorado State University, Fort Collins, CO 80523, USA. E-mail: joe.zadrozny@colostate.edu

^b X-ray Science Division, Argonne National Laboratory, Argonne, Illinois 60439, USA

† Footnotes relating to the title and/or authors should appear here.

Electronic Supplementary Information (ESI) available: Additional sample preparation details, characterization data, x-ray absorption data, and computational details. See DOI: 10.1039/x0xx00000x

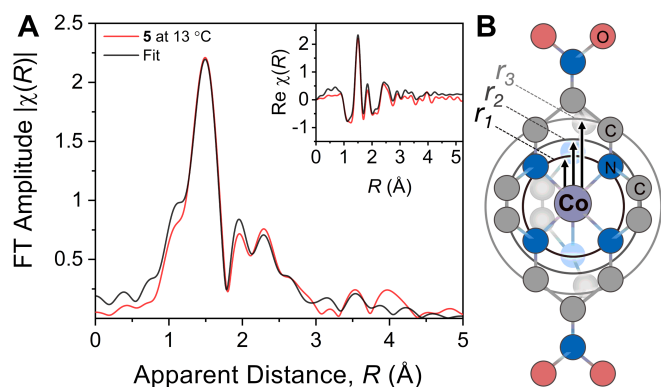


Fig. 2. (A) Radial structure function plot shown as Fourier Transform EXAFS data (red) of **5** at 13 °C and fit (black) with k^2 -weighting over k -range of 2 – 12 Å⁻¹. Inset: Fit of real part of the FT EXAFS data. (B) Highlighted intramolecular atomic single scattering distances of **5** from the primary Co–N₆ shell r_1 , followed by second and third shells of methylene carbon atoms r_2 and r_3 , respectively.

angles, could be adjusting the ⁵⁹Co δ as a function of temperature in addition to simple bond expansion. Yet, to the best of our knowledge, no studies to directly correlate variable-temperature structure to ⁵⁹Co $\Delta\delta/\Delta T$ have ever been performed.

Herein, we report a variable-temperature structural study of five cobalt(III) complexes (Fig. S1) via extended X-ray absorption fine-structure (EXAFS) spectroscopic measurements of [Co(NH₃)₆]Cl₃ (**1**),¹⁸ [Co(en)₃]Cl₃ (**2**) (en = ethylenediamine),¹⁹ [Co(tn)₃]Cl₃ (**3**) (tn = trimethylenediamine),²⁰ [Co(tame)₂]Cl₃ (**4**) (tame = 1,1,1-tris(aminomethyl)ethane),²¹ and [Co(diNOsar)]Cl₃ (**5**) (diNOsar = dinitrosarcophagine).²² EXAFS spectroscopy is a widely employed technique for elucidating the coordination spheres of metal ions in solution-phase samples.^{23–27} Here, we apply this spectroscopic technique for the first time in studying the actual structural changes that govern ⁵⁹Co $\Delta\delta/\Delta T$. The studied complexes were selected to provide a structural progression of increasing connectivity between the donor atoms and to best compare structural changes with previously determined values of $\Delta\delta/\Delta T$.¹¹ Herein, we find that the magnitude of change in Co–N bond distance (Δr_1 in Fig. 1) does not directly correlate to $\Delta\delta/\Delta T$. Instead, computational analyses guided by the EXAFS results indicate structurally unique distortions occur, enabled by chelating and macrocyclic ligands.

Results and Discussion

Fluorescence detection was used to measure the Co K -edge EXAFS spectra of **1–5**. The EXAFS results from photoelectrons scattered between the central absorbing cobalt ion and nearby atoms and can therefore be used to elucidate interatomic distances within the molecules. For each complex, Fourier transform (FT) analysis of EXAFS spectra yielded an intense primary feature at apparent R values of 1.5–2.0 Å and many less-intense features at greater R values (Fig. 2A). The highest intensity peaks stem from single scattering paths from the immediate coordination shell of the cobalt ion (r_1 of nitrogen on

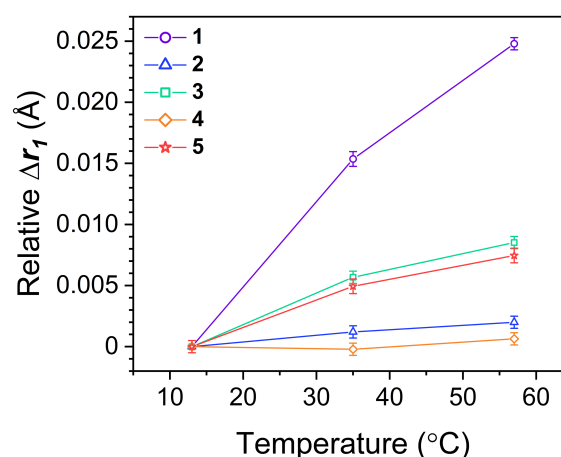


Fig. 3. Relative change in Co–N₆ bond length r_1 (Δr_1 , Å) for solution-phase samples of **1–5** across a 13–57 °C temperature range with error bars at each measurement.

5 in Fig. 2B). Additional single scattering paths occur at longer distances from the cobalt ion, such as from ligand-based carbon atoms (e.g. r_2 and r_3 of ethylene carbons on **5**, Fig. 2B) and show up between R values of 2.2–3.3 Å. Finally, proximate counterions (e.g. a Cl⁻) or other molecules in the solvent cage produce variable features at the highest R values.

The EXAFS spectra were fit to extract Co–N bond distances using the reported crystal structures of **1–5**. The resulting determined distances largely agree with reported bond lengths from the experimental literature structure models. For example, the EXAFS-reported Co–N bond length of **5** at 13 °C is $r_1 = 1.9701(5)$ Å, which is within ± 0.012 Å to the reported structure of **5** at 1.982 Å.²² The correlation between EXAFS and diffraction data also holds for **1–4**, where r_1 values are in agreement with reported Co–N bond lengths (1.96–1.99 Å).^{18–22} Distances to secondary and tertiary atomic shells of **5** at 13 °C are $r_2 = 2.7984(5)$ Å and $r_3 = 2.9777(5)$ Å. These values are also in approximate agreement with the Co···C_{ligand} distances of the crystal structure at 2.815 and 2.994 Å. Note that even though r_1 , r_2 , and r_3 are close to the crystal structure values, slight differences are to be expected given that these data were recorded in solution. Finally, the data are in agreement with prior single-temperature-only EXAFS (and X-ray absorption near-edge structure) investigations.^{28–30}

Variable-temperature EXAFS studies were performed to study the temperature-dependence of the determined Co–N distances and other structural features in **1–5**. These measurements were conducted in Milli-Q deionized water over a ~ 50 °C temperature window at three temperatures, 13, 35, and 57 °C. Structural analyses (e.g. those for **5** in Fig. 2) were made at each temperature measurement, providing a determination of relative Co–N bond distance as a function of temperature. Fitting these spectra using the reported crystal structures as starting points enabled us to probe the temperature dependence of the first coordination shells in **1–5**.

The fits show a complex set of increasing scattering path distances with temperature over the 13–57 °C range (Fig. S2–S16). Importantly, an analysis of temperature-driven bond distance shows an increase in r_1 (the Co–N₆ primary

coordination sphere) with increasing temperature. For **5**, we determined an increase in the Co–N bond distance from 1.9701(5) Å at 13 °C, to 1.9751(6) Å at 35 °C, and finally to 1.9776(6) Å at 57 °C (Fig. 3). Similar temperature-sensitive behaviour of the primary coordination sphere is seen in **1-4** (Table S1). At the lowest temperature, 13 °C measurement, Co–N₆ coordination distances are $r_1 = 1.9588(5)$ Å for **1**, 1.9694(5) Å for **2**, 1.9825(5) Å for **3**, and 1.9700(5) Å for **4**. In the highest-temperature, 57 °C measurement, the Co–N₆ distances are expanded: $r_1 = 1.9836(5)$ Å for **1**, 1.9714(5) Å for **2**, 1.9910(5) Å for **3**, and 1.9707(5) Å for **4** (Table S1). The total changes in the Co–N atomic distances over the ~50 °C range are therefore $\Delta r_1 = +0.0248(6)$, $+0.0020(5)$, $+0.0085(5)$, $+0.0007(5)$, and $+0.0075(6)$ Å for **1-5**, respectively (Fig. 3). These data indicate the highest change in Co–N bond distances for **1**, in which all N-donor atoms are monodentate NH₃ ligands. Significantly less bond distance variation is observed for **2-5**, which contain chelating or macrocyclic ligands. These variations may seem minute from an absolute comparison to crystal structure models where precision of atomic distances is commonly difficult to resolve below ~0.001 Å. Yet, *relative* changes in atomic distances are highly accurate when determined by EXAFS with the appropriate fitting methods (see ESI and Table S3). We report relative uncertainties as low as ± 0.0005 Å as deduced from the EXAFS fits parameters, including noise and energy instability.^{31–36}

Similar to the Co–N scattering paths, which expand for all compounds **1-5**, the scattering paths from carbon atoms in chelating ligand backbones (e.g. r_2 and r_3 for **5**) also increase with temperature (Tables S4–S15). For **2**, the distances of carbon ligand atoms increase over a range of $+0.0029(6)$ Å. For **3**, there are two unique carbon-atom single scattering paths which arise from the carbons adjacent to the N-donor atoms (r_2), and the bridging methylene carbon atoms (r_3), between them. With increasing temperature, both of these paths increase by $\Delta r_2 = +0.0130(6)$ Å and $\Delta r_3 = +0.0145(6)$ Å, respectively. For **4**, there are individual single scattering paths to three different shells of ligand carbon atoms. At increasing distances, these paths originate from the methylene carbon atoms bound to the N-donor atoms (r_2), the apical quaternary carbons of each tame ligand (r_3), and finally the axial methyl carbons (r_4). For these carbon atoms, all paths increase by $+0.0010(5)$ Å for Δr_2 and Δr_3 and $+0.0015(5)$ Å for Δr_4 . Finally, for **5**, there are three independent single scattering paths arising from the carbon atoms of the ethylenediamine fragments (r_2), the apical methylene carbons (r_3), and the NO₂-functionalized quaternary carbons (r_4). Similar to changes in atomic ligand displacements of other complexes, these distances all increase with increasing temperature. For **5**, the differences between the high and low temperature measurements are a positive increase of $+0.0110(6)$ Å for Δr_2 , Δr_3 and Δr_4 .

The EXAFS data provide some support the individual models of Jameson et al. and Benedek et al. while simultaneously suggesting a richer picture of structural dynamics responsible for $\Delta\delta/\Delta T$.^{12,14} For example, the Δr_1 values determined for **1-5** vary within 0.0006 to 0.0256 Å over 13–57 °C. Most importantly, however, the observed variation in structure is inconsistent

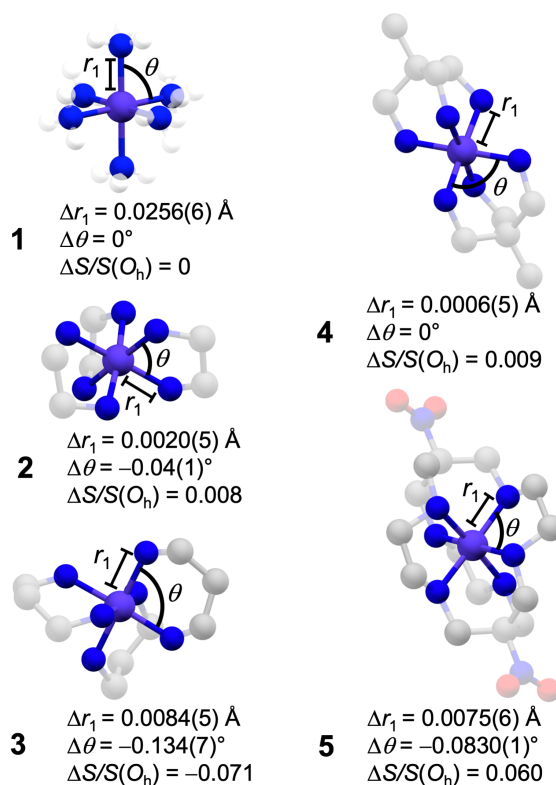


Fig. 4. Comparative geometric distortions of **1-5** from 13–57 °C represented by the change in Co–N bond length Δr_1 , average chelate bite angle $\Delta\theta$, and relative deviations from O_h geometry $\Delta S/S(O_h)$ (relative to the 13 °C $S(O_h)$ value). Purple and blue atoms represent Co and N atoms in the first coordination shell, respectively. Faded blue, red, gray, and white spheres represent N, O, C, and H atoms in the ligand backbones for the shown molecules. Hydrogens on structures **2-5** are omitted for clarity.

with the previous analyses of $\Delta\delta/\Delta T$. For **1-5**, the $\Delta\delta/\Delta T$ varies as 1.44(2), 1.38(1), 1.30(2), 1.71(1), and 2.04(2) ppm/°C, respectively.¹¹ This trend in $\Delta\delta/\Delta T$ is **3** < **2** < **1** < **4** < **5**, with the macrocyclic sarcophagine ligand engendering the highest temperature dependence of ⁵⁹Co δ . The trend in $\Delta\delta/\Delta T$ does not correspond to Δr_1 over the same temperature window, which varies as **4** < **2** < **5** < **3** < **1**.

A straightforward method to reconcile the disagreement between $\Delta\delta/\Delta T$ and $\Delta r_1/\Delta T$ is to conclude that the change in Co–N bond distance is not the sole design criterion for enhancing $\Delta\delta/\Delta T$ for a transition-metal nuclear spin. Note that the chemical shift of octahedral ⁵⁹Co nuclei stems directly the ligand-field splitting Δ_o .^{37–40} Hence, *any* potential temperature-dependent structural changes that affect metal-ligand overlap (and hence modulate Δ_o) could impact δ . As represented in this work, the lacking correspondence between Δr_1 and $\Delta\delta/\Delta T$ could signal complex structural dynamics beyond simple Co–N expansion, e.g. changes in N–Co–N bond angles.

Computational analyses of the structural variations in **1-5** were performed to gain deeper insight into the motions that accompany lengthening of the Co–N bonds (Fig. 4). We used the ω B97xd DTF functional⁴¹ with the 6-311+g* basis set⁴² to compute the optimized geometries of **1-5** at the lowest and

highest temperatures of EXAFS measurement while restraining the Co–N distances to those determined from r_1 (see SI). All other structural distances and angles were then allowed to freely refine during optimization. These computations reflect complex structural dynamics as a function of temperature for the macrocyclic and chelated complexed **2-5** (Fig. 4). For example, in **2** and **3** the ligand bite angles decrease with increasing Co–N bond length, by $-0.04(1)^\circ$ for **2** and $-0.134(7)^\circ$ for **3** (Tables S19–S20). This change is also seen for the ethylene-bridged amines in **5**, which change by $-0.0830(1)^\circ$ for **5** (Table S21). Complexes **2** and **5** share ethylene-bridged donor atoms, yet the bite angles change more significantly in **5** which may stem from the additional interconnectivity of the macrocyclic ligand. The least amount of *average* change in chelate bite angle (over the whole molecule) is exhibited by the tridentate ligand of **4** despite individual N–Co–N bite angles changing by 0.018° (Fig. S17). In contrast, **1**, wherein no inter-ligand connectivity is present, exhibits a simple expansion of Co–N distances with increasing temperature.

Changes in the optimized coordination geometries as a function of temperature were also investigated via SHAPE analysis.^{43,44} SHAPE is a continuous symmetry measurement tool that enables comparisons of geometric distortions between two idealized geometries.⁴⁵ We chose octahedral and trigonal-prismatic idealized structures as the two points of comparison, given the possible enantiomeric and diastereomeric configurations of **2-5**.^{46–49} SHAPE analyses are used to evaluate how close a particular structure is to idealized symmetry to octahedral or trigonal prismatic geometries. A shape measure, S , of 0 for a given geometry indicates a perfect match, whereas a large S highlights strong disagreement in the structural assignment.

The analyses revealed two key structural features in **1-5**. First, the immediate coordination environments of **1-5** are better described as O_h symmetry than D_{3h} trigonal-prismatic symmetry, since $S(O_h)$ is < 0.3 for **1-5** in contrast to $S(D_{3h})$, which is > 10 for **1-5** (Tables S22–S23). Second, the variable-temperature analyses show small but unique structural deviations in **1-5** with increasing temperatures. For the temperature-specific optimized structures of **1**, for example, SHAPE analysis reveals no deviation from O_h symmetry with increasing temperature. This lack of change is represented by zero change in the shape measure for the O_h geometry relative to the $S(O_h)$ at 13°C , $\Delta S(O_h)/S(O_h)$. In contrast, **2-5** exhibit distortions of (**3** approaches O_h symmetry with increasing temperature, represented by $\Delta S/S(O_h) = -0.071$. Complex **4** shows a comparable scale of change to **2**, distorting away from O_h symmetry ($\Delta S/S(O_h) = 0.009$) with warming, while **5** shows the greatest deviation away from O_h symmetry ($\Delta S/S(O_h) = 0.060$). With increasing temperature, **5** also shows the strongest shift towards trigonal-prismatic D_{3h} symmetry in the series of studied complexes ($\Delta S/S(D_{3h}) = -0.005$) (Table S22–S23).

These results highlight two important points for future NMR thermometer development. First, the observed distortions show that relatively small structural changes have significant impacts on ^{59}Co NMR chemical shifts. Hence, the data provide important experimental corroboration of the initial theoretical

arguments by Benedek and Jameson.^{12,14} Second, the changes highlight that $\Delta\delta/\Delta T$ in macrocyclic and chelated ligand systems cannot be accounted for by unidirectional M–L bond displacements alone.

A new molecular design strategy is potentially underlined in this latter point. If changes in M–L bond distances are not the essential molecular feature dictating $\Delta\delta/\Delta T$, then the changes in L–M–L angles seem like the next-best feature to tune. Here, one could envision harnessing structural strain in chelating and macrocyclic ligands to spring-load changes in bond distances *and* angles as a function of temperature. Studies evidencing significant strain in chelate and macrocyclic ligands are abundant in the literature,^{50–53} underlining the promise of potentially harnessing this feature in metal complexes with significant chemical stability *in vivo*.

Conclusions

The foregoing study is the first systematic structural examination of ^{59}Co $\Delta\delta/\Delta T$ through variable-temperature EXAFS measurements. Importantly, we find that temperature-dependent changes in Co–N bond distances Δr_1 for **1-5** do not directly follow $\Delta\delta/\Delta T$ in these complexes. Indeed, following computational analyses, the foregoing data reveal a new picture of ^{59}Co δ thermometry that involves changes in both M–L bond distances and angles between donor atoms. Importantly, the results suggest future strategies to harness molecular strain to engender higher $\Delta\delta/\Delta T$. In the long run, this concept will be employed in hybrid synthetic/theoretical studies to design macrocyclic complexes with high $\Delta\delta/\Delta T$.

Conflicts of interest

There are no conflicts to declare.

Acknowledgements

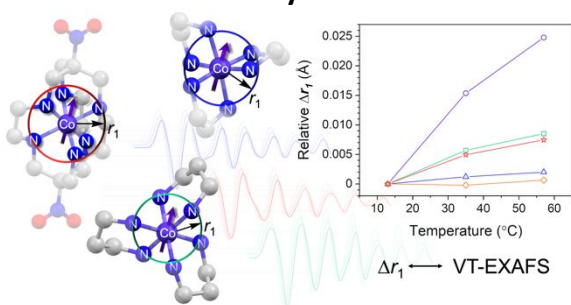
We acknowledge Mr. Justin Joyce for useful discussions and experimental assistance. This research was performed with the support of Colorado State University (CSU) and the NIH (R21-EB027293). This research was performed at beamline 9-BM of the Advanced Photon Source, a U.S. Department of Energy (DOE) Office of Science User Facility operated for the DOE Office of Science by Argonne National Laboratory under Contract No. DE-AC02-06CH11357. Computational resources are enabled by the Catalysis Collaboratory for Light-activated Earth Abundant Reagents (C-CLEAR), which is supported by the National Science Foundation (NSF) and the Environmental Protection Agency through the Networks for Sustainable Molecular Design and Synthesis (CHE-1339674) at Colorado State University, Fort Collins.

Notes and References

- 1 V. Rieke, K. B. Pauly, *J. Magn. Reson. Imaging*, 2008, **27**, 376.

- 2 B. Denis de Senneville, B. Quesson, C. T. W. Moonen, *Int. J. Hyperthermia*, 2005, **21**, 515.
- 3 H. Odéen, D. L. Parker, *Prog. Nucl. Magn. Reson. Spectrosc.*, 2019, **110**, 34.
- 4 J. Yuan, C.-S. Mei, L. P. Panych, N. J. McDonald, B. Madore, *Quant. Imaging Med. Surg.*, 2012, **2**, 21.
- 5 H. Tseng, S.-E. Lin, Y.-L. Chang, M.-H. Chen, S.-H. Hung, *Exp. Ther. Med.*, 2016, **11**, 763.
- 6 W. G. Proctor, F. C. Yu, *Phys. Rev.*, 1951, **81**, 20.
- 7 R. Freeman, G. R. Murray, R. E. Richards, *Proc. R. Soc. Lond. Ser. Math. Phys. Sci.*, 1957, **242**, 455.
- 8 J. C. C. Chan, S. C. F. Au-Yeung, Cobalt-59 NMR Spectroscopy. *Ann. Rep. NMR Spectrosc.*, 2000, 41, pp 1–54.
- 9 G. C. Levy, J. Terry Bailey, D. A. Wright, *J. Magn. Reson.*, 1980, **37**, 353.
- 10 L. Leyssens, B. Vinck, C. Van Der Straeten, F. Wuyts, L. Maes, *Toxicology*, 2017, **387**, 43.
- 11 T. M. Ozvat, M. E. Peña, J. M. Zadrozny, *Chem. Sci.*, 2019, **10**, 6727.
- 12 C. J. Jameson, D. Rehder, M. Hoch, *J. Am. Chem. Soc.*, 1987, **109**, 2589.
- 13 C. J. Jameson, *J. Am. Chem. Soc.*, 1987, **109**, 9, 2586.
- 14 G. B. Benedek, R. Englman, J. A. Armstrong, *J. Chem. Phys.*, 1963, **39**, 12, 3349.
- 15 D. G. Gillies, L. H. Sutcliffe, A. J. Williams, *Magn. Reson. Chem.*, 2002, **40**, 57.
- 16 M. R., Bendall, D. M. Doddrell, *Aust. J. Chem.*, 1978, **31**, 1141.
- 17 H.-Jörg Osten, C. J. Jameson, *J. Chem. Phys.*, 1985, **82**, 4595.
- 18 G. J. Kruger, E. C. Reynhardt, *Acta Crystallogr. Sect. B*, 1978, **34**, 915.
- 19 K. Nakatsu, Y. Saito, H. Kuroya, *Bull. Chem. Soc. Jpn.*, 1956, **29**, 428.
- 20 R. Nagao, F. Marumo, Y. Saito, *Acta Crystallogr. Sect. B*, 1973, **29**, 2438.
- 21 R. J. Geue, M. R. Snow, *Inorg. Chem.*, 1977, **16**, 231.
- 22 I. Clark, R. Geue, L. Engelhardt, J. Harrowfield, A. Sargeson, A. White, *Aust. J. Chem.*, 1993, **46**, 1485.
- 23 T. M. Seward, C. M. B. Henderson, J. M. Charnock, B. R. Dobson, *Geochim. Cosmochim. Acta*, 1996, **60**, 2273.
- 24 P. Frank, M. Benfatto, M. Qayyam, B. Hedman, K. O. Hodgson, *J. Chem. Phys.*, 2015, **142**, 084310.
- 25 C. Garino, E. Borfecchia, R. Gobetto, J. A. van Bokhoven, C. Lamberti, *Coord. Chem. Rev.*, 2014, **277–278**, 130–186.
- 26 D. T. Bowron, S. Diaz Moreno, *Coord. Chem. Rev.*, 2014, **277–278**, 2.
- 27 J. E. Penner-Hahn, X-Ray Absorption Spectroscopy, *Encyclopedia of Life Sciences*; John Wiley & Sons, Ltd. Ed., Chichester, UK, 2005; pp 1–4.
- 28 W.-K. Chen, J. Chen, P. M. Rentzepis, *J. Phys. Chem. B*, 2013, **117**, 4332–4339.
- 29 T. Akai, M. Okuda, K. Horiuchi, J. Matsuura, Y. Koike, M. Yimagawa, T. Fujikawa, *Jpn. J. Appl. Phys.*, 1994, **33**, 6360–6367.
- 30 P. D. Bonnitcho, M. D. Hall, C. K. Underwood, G. J. Foran, M. Zhang, P. J. Beale, T. W. Hambley, *J. Inorg. Biochem.*, 2006, **100**, 963–971.
- 31 J. Purans, J. Timoshenko, A. Kuzmin, G. Dalba, P. Fornasini, R. Grisenti, N. D. Afify, F. Rocca, S. De Panfilis, I. Ozhogin, *J. Phys. Conf. Ser.*, 2009, **190**, 012063.
- 32 J. Purans, N. D. Afify, G. Dalba, R. Grisenti, S. De Panfilis, A. Kuzmin, V. I. Ozhogin, F. Rocca, A. Sanson, S. I. Tiutiunnikov, P. Fornasini, *Phys. Rev. Lett.*, 2008, **100**, 055901.
- 33 J. Purans, G. Dalba, P. Fornasini, A. Kuzmin, S. De Panfilis, F. Rocca, *AIP Conference Proceedings*; AIP: Stanford, California (USA), 2007; Vol. 882, pp 422–424.
- 34 G. Dalba, P. Fornasini, R. Grisenti, J. Purans, *Phys. Rev. Lett.*, 1999, **82**, 4240.
- 35 N. Adb el All, G. Dalba, D. Diop, P. Fornasini, R. Grisenti, O. Mathon, F. Rocca, B. Thiodjio Sendja, M. Vaccari, *J. Phys.: Condens. Matter*, 2012, **24**, 115403.
- 36 Sharma, M.; Tripathi, J.; Mishra, A.; Yadav, A. K.; Jha, S. N.; Shrivastava, B. D. *Mater. Today: Proc.*, 2019, **12**, 614.
- 37 J. S. Griffith, L. E. Orgel, *Trans. Faraday Soc.*, 1957, **53**, 601.
- 38 R. Bramley, M. Brorson, A. M. Sargeson, C. E. Schäffer, *J. Am. Chem. Soc.*, 1985, **107**, 2780.
- 39 N. Juranić, *Inorg. Chem.*, 1980, **19**, 1093.
- 40 N. Juranić, *J. Chem. Phys.*, 1981, **74**, 3690.
- 41 F. Neese, *J. Chem. Phys.*, 2003, **119**, 9428.
- 42 R. Krishnan, J. S. Binkley, R. Seeger, J. A. Pople, *J. Chem. Phys.*, 1980, **72**, 650.
- 43 S. Alvarez, D. Avnir, M. Lluell, M. Pinsky, *New J. Chem.*, 2002, **26**, 996.
- 44 S. Alvarez, P. Alemany, D. Casanova, J. Cirera, M. Lluell, D. Avnir, *Coord. Chem. Rev.*, 2005, **249**, 1693.
- 45 M. Pinsky, D. Avnir, *Inorg. Chem.*, 1998, **37**, 5575.
- 46 R. J. Geue, A. J. Hendry, A. M. Sargeson, *J. Chem. Soc. Chem. Commun.*, 1989, 1646.
- 47 S. T. Spees, L. J. Durham, A. M. Sargeson, *Inorg. Chem.*, 1966, **5**, 2103.
- 48 P. Comba, I. I. Creaser, L. R. Gahan, J. M. Harrowfield, G. A. Lawrance, L. L. Martin, A. W. H. Mau, A. M. Sargeson, W. H. F. Sasse, M. R. Snow, *Inorg. Chem.*, 1986, **25**, 384.
- 49 P. Comba, A. M. Sargeson, L. M. Engelhardt, J. Harrowfield, A. H. White, E. Horn, M. R. Snow, *Inorg. Chem.*, 1985, **24**, 2325.
- 50 P. Comba, *Inorg. Chem.*, 1989, **28**, 426.
- 51 J. Harrowfield, *Supramol. Chem.*, 2006, **18**, 125.
- 52 J. F. Endicott, G. R. Brubaker, T. Ramasami, K. Kumar, K. Dwarakanath, J. Cassel, D. Johnson, *Inorg. Chem.*, 1983, **22**, 3754.
- 53 A. M. Bond, T. W. Hambley, M. R. Snow, *Inorg. Chem.*, 1985, **24**, 1920.

Table of Contents Entry



EXAFS spectroscopy was used to study the temperature-dependent molecular structures of a series of Cobalt-59 NMR thermometers.